Investigation of a Microwave Data Telemetry Link for a Retinal Prosthesis

Keyoor Gosalia, *Student Member, IEEE*, Gianluca Lazzi, *Senior Member, IEEE*, and Mark Humayun, *Member, IEEE*

***Abstract*—In this paper, we investigate a novel approach of establishing a data telemetry link for a dual-unit retinal prosthesis at microwave frequencies (1.45 and 2.45 GHz) using a pair of microstrip patch antennas. Appropriately sized extraocular (25×25 mm) and intraocular (6×6 mm) antennas are designed to operate at both the frequencies using the finite-difference time-domain method, and the coupling between them is examined computationally in the presence of a 0.25-mm resolution human-head model. Good agreement between numerical and experimental coupling results is shown and it is observed that the eyeball acts as a dielectric lens for the implanted antenna, thus improving the coupling between the extraocular and intraocular antennas. Specific absorption rate (SAR) computations are also performed at both the frequencies, and the peak 1-g SAR value is calculated. Detailed analysis of the design issues of the antennas, results of the numerical and experimental coupling measurements, and SAR calculations are presented.**

***Index Terms*—Antenna coupling, data telemetry, dosimetry, retinal prosthesis.**

I. Introduction

PROGRESSIVE loss of light-sensitive photoreceptors of the retina lead to a severe loss of vision in patients suffering from incurable retinal diseases like retinitis pigmentosa (RP) and age-related macular degeneration (AMD). In a healthy retina, photoreceptors generate a neural signal in response to incident light, which is further processed by the bipolar and ganglion cells before being delivered to the optical nerve and visual cortex. In patients suffering from RP and AMD, photoreceptors are almost completely absent, but the cells to which they normally synapse (the bipolar and ganglion cells) survive at high rates [1].

It has been clinically demonstrated that artificial electrical stimulation of the surviving ganglion cells can elicit visual perception in patients [2], [3]. An implantable retinal prosthesis can be designed to replace the functionality of the missing photoreceptors by directly providing electrical stimulation to the next surviving layer of retina (the bipolar and/or ganglion cell layer), thus restoring partial vision in such patients. Two approaches have mainly been proposed to achieve artificial electrical stimulation, and they differ in the positioning of their electrode array [4]. In the epiretinal approach, the implant array is positioned on the surface of the inner retina [5]–[7], while in the subretinal approach, the device is implanted between the pigment epithelial layer and the outer layer of the retina [8], [9]. An entirely different approach to evoke visual perception-by direct stimulation of the visual cortex is proposed in [10]. An extensive review of these approaches is provided in [3]. It must be mentioned that recent work [11] has shown that, in retinas of patients suffering from RP and AMD, along with the loss of photoreceptors, there could be a considerable degeneration and reorganization of the retinal structure itself, which might impact the artificial stimulation.

The retinal prosthesis system considered here is a dual-unit epiretinal device with an extraocular and implanted intraocular unit. The extraocular unit is comprised of the image capturing and processing chips, an amplifier, and the primary coil. The intraocular unit contains the secondary coil, rectifier and signal-processing chips, and an electrode array [5]. Conventionally, power and data communication between the external and internal units of such prosthetic devices has been accomplished by a single low-frequency (2–10 MHz) inductive link between a pair of coils. In such an approach, the data signal modulates the low-frequency power carrier. Recent work [12] shows that a low-frequency inductive link can have sufficient bandwidth for a 2–3-Mb/s data signal required for a 32×32 electrode array (for a stimulation frequency of 60 Hz). Efforts are underway to manufacture significantly more dense, ultra-thin, and flexible electrode arrays, which fit neatly into the curvature of the retina in the eyeball. It is anticipated that the data signal for such dense electrode arrays will require a much larger bandwidth. In such cases, mutually exclusive power and data transfer can prove useful in providing a solution to transfer power at low frequencies while establishing a high-bandwidth data link at microwave frequencies. Data communication at microwave frequencies (1–3 GHz) using a pair of external and internal microstrip patch antennas can provide higher bandwidth and is a viable alternative, as computationally demonstrated in [13].

In this paper, the feasibility of a microwave data telemetry link employing an extraocular and implanted intraocular antenna is demonstrated both computationally, as well as experimentally (with the use of phantoms) in two frequency bands at 1.45 and 2.45 GHz. Appropriately sized microstrip patch antennas are designed and implemented to operate as extraocular and intraocular antennas at both frequency bands [14]. The influence of the head and eye on the coupling between the antennas is characterized, and it is observed that the eyeball acts as a dielectric lens and improves coupling performance. Computationally, the data link is characterized for a maximum transmitted power of 50 mW. Considering the worst case coupling

Manuscript received October 9, 2003; revised April 1, 2004. This work was supported in part by the National Science Foundation under CAREER Award ECS-0091599, Grant EEC-0310723, and Grant ECS-0335537, and by the Whitaker Foundation under Grant RG-00-0298.

K. Gosalia and G. Lazzi are with the Department of Electrical and Computer Engineering, North Carolina State University, Raleigh, NC 27695-7911 USA.

M. Humayun is with the Doheny Eye Institute, Keck School of Medicine, University of Southern California, Los Angeles, CA 90033 USA.

Digital Object Identifier 10.1109/TMTT.2004.832007

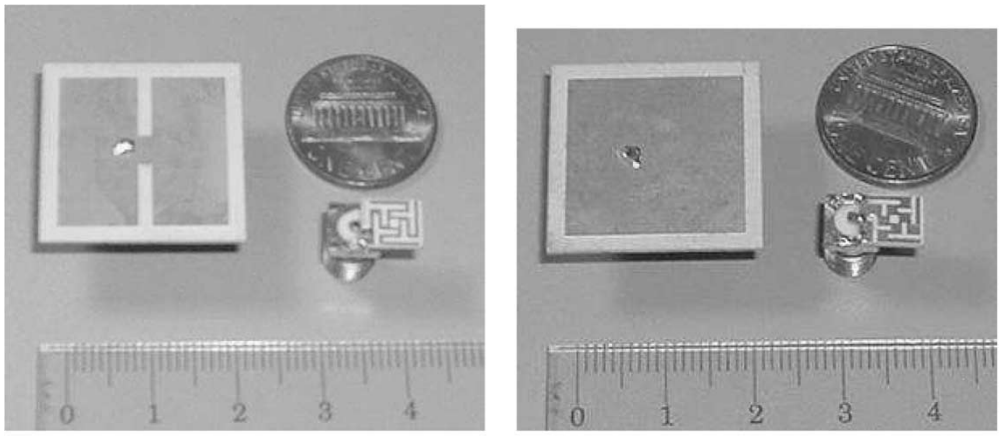

(a) (b)

Fig. 1. Photographs showing the fabricated extraocular and intraocular antennas at both the frequency bands. (a) 1.45 GHz. (b) 2.45 GHz.

efficiency between the antennas (−45 dB at 1.45 GHz), and the extremely sensitive RF front-end receivers available (−50 dBm and higher), the extraocular antenna is not expected to transmit more than 50 mW. Hence, the specific absorption rate (SAR) computations are performed for a radiated power of 50 mW in both the frequency bands. The evaluated SAR values are within the safety limits specified in the IEEE/American National Standards Institute (ANSI) Standard [15].

This paper is organized as follows. Section II describes the antenna design and implementation issues in both frequency bands. A brief description of the head model used and the computational method and domain employed is provided in Section III. The setup for experimental measurements is described in Section IV. The influence of the eye model on the antenna characteristics and the corrective measures employed are discussed in Section V. Coupling results and SAR computations at both frequency bands are presented in Section VI and, finally, Section VII presents conclusions.

II. Antenna Design

Owing to the nature of the application, the transmitting and receiving antennas must be very compact, robust, and lightweight. Thus, microstrip patch antennas [16], [17] were selected. The extraocular antenna was designed to have dimensions within 25×25 mm to fit on a pair of glasses to be worn by the patient, while the intraocular antenna was to be designed with dimensions less than 6×6 mm to accommodate it within the ciliary muscles of the eye (held by the zonules in place of the lens)—approximately 6–7 mm posterior to the cornea. At both the frequency bands, a pair of extraocular and intraocular antennas were designed within the above-stated dimensions using an in-house finite-difference time-domain (FDTD) code. For this study, all the antennas are designed with a high dielectric constant of $\varepsilon_r = 9.2$ and a thickness of $h = 0.5$ mm.

A. Frequency Band at 1.45 GHz

Several size-reduction techniques—as outlined comprehensively in [18]—were employed to design the compact extraocular and intraocular antennas. The extraocular antenna was designed by incorporating a pair of vertical slots along the nonradiating edges of the antenna. By varying the length of the slots, the desired compactness was achieved and the antenna dimensions were restricted to $25 \times 25 \times 0.5$ mm. For the intraocular antenna, to facilitate its embedding in the eye ball, it was essential to restrict its size approximately to within $6 \times 6 \times 0.5$ mm. A symmetric array of slots were etched out from the surface and a single shorting post was used near the feed point to resonate and match the extremely compact intraocular antenna. The implemented extraocular and intraocular antennas are shown in Fig. 1(a), while Fig. 2(a) details the design parameters for the intraocular antenna.

B. Frequency Band at 2.45 GHz

For the same dimensions of the extraocular and intraocular antennas, the degree of compactness required at 2.45 GHz is less than that required at 1.45 GHz. Thus, with dimensions of $25 \times 25 \times 0.5$ mm, a simple patch antenna was designed to operate as the extraocular antenna at 2.45 GHz. The array of slots used on the 2.45-GHz intraocular antenna was identical to that of the 1.45-GHz intraocular antenna, but since the required compactness was lower, the length of the slots was reduced for the 2.45-GHz intraocular antenna. Also, two shorting posts were introduced symmetrically with respect to the feed location to achieve matching for the 2.45-GHz intraocular antenna. Fig. 1(b) shows a photograph of implemented extraocular and intraocular antennas in this frequency band. Fig. 2(b) shows the design parameters for the intraocular antenna. The parameter specifics for Fig. 2(a) and (b) are listed in Table I.

As seen from Fig. 2(a) and (b), the proposed designs facilitated slight variations in the width of the shorting post/s and in the length of slots. Such modifications had to be incorporated at both frequency bands (both in FDTD simulations, as well as after implementation) to match the intraocular antenna's resonance frequency to that of the extraocular antenna. Also, due to tolerances involved during actual fabrication, the realized antennas resonated at 1.4 and 2.37 GHz instead of the computationally designed 1.45 and 2.45 GHz, respectively. For the remainder of this paper, to maintain consistency of notation, the

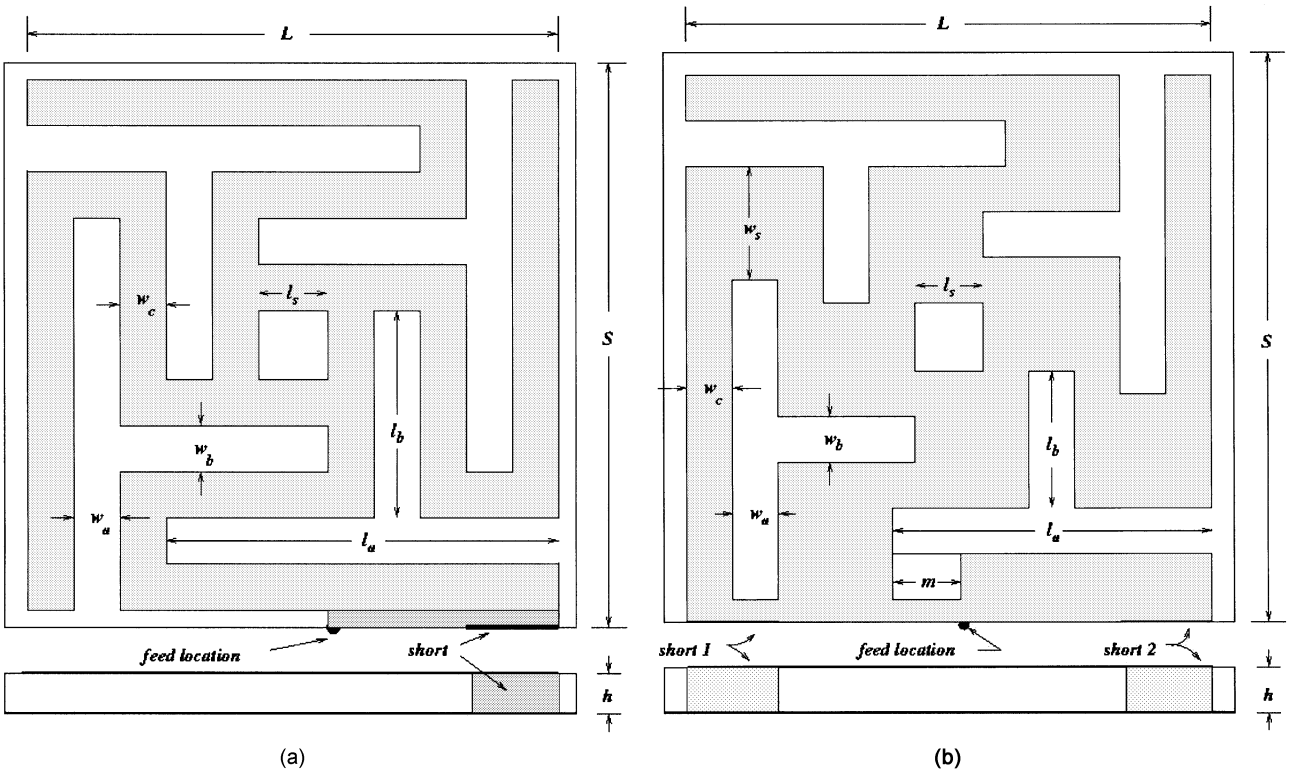

Fig. 2. Design parameters for the intraocular antennas at both frequency bands. (a) 1.45 GHz. (b) 2.45 GHz.

TABLE I
PARAMETERS DEFINED IN FIG. 2 FOR THE PROPOSED INTRAOCULAR ANTENNA DESIGN AT BOTH THE FREQUENCY BANDS (ALL DIMENSIONS IN MILLIMETERS)

Intraocular antenna	S	L	l_a	l_b	l_s	w_a	w_b	w_c	w_s	m
1.45 GHz	6.25	5.75	4.25	2.25	0.75	0.5	0.5	0.5	–	–
2.45 GHz	6.25	5.75	3.5	1.5	0.75	0.5	0.5	0.5	1.25	0.75

antennas will be referred to as belonging to the corresponding 1.45- or the 2.45-GHz band, and it should be understood that, for the experimental results shown, the implemented antennas actually operated at 1.4 and 2.37 GHz.

III. HUMAN-HEAD MODEL AND FDTD MODELING

The data for the head model was obtained in the form of cross-sectional slices of 1-mm resolution from the National Library of Medicine (NLM) "Visible Man Project."[1] In this application, since it was essential to represent the tissues of the eye and head with a high degree of detail, the head model was discretized further—to reach a spatial resolution of 0.25 mm (64 times the original one) using a method of interpolation in all three dimensions [13]. The detailed features of the eye were represented as described in [5], and the dielectric properties of the body tissues at the frequencies of 1.45 and 2.45 GHz were obtained from the online database compiled by Gabriel.[2] The dielectric properties of those tissues not explicitly available from the online database were obtained as mentioned in [5]. For the coupling performance and SAR computations, a portion of this head model was extracted and used in the computational domain, as shown in Fig. 3(a).

A three-dimensional D-H formulation of the FDTD method [19] has been employed with a uniform cell grid of 0.25-mm resolution to compute the performance of the data telemetry link in the presence of the head model. A material-independent perfectly matched layer (PML) is used as an absorbing boundary condition so that the model can be immersed in the PML layers, as mentioned in [20]. The lens of the eye is removed from the head model (to be consistent with the actual intended surgical procedure) and the intraocular antenna is encapsulated with a thin 1-mm-thick insulating layer and embedded in its place as shown in the cross-sectional image of Fig. 3(b). The extraocular antenna is modeled corresponding to its position on a pair of glasses at a distance of approximately 25 mm from the intraocular embedded antenna. At both the frequency bands, FDTD computations were performed to determine the coupling between the extraocular and implanted antennas in these positions. SAR computations were also carried out within the same computational model at 1.45 and 2.45 GHz to determine the extent of power deposition in the head and eye tissues due to operation of the data telemetry link.

[1]The National Library of Medicine, Bethesda, MD [Online]. Available: http://www.nlm.nih.gov/research/visible/visible_human.html, 2000.

[2]Dielectric properties of body tissue. [Online]. Available: http://safeemf.iroe.fi.cnr.it/tissprop/

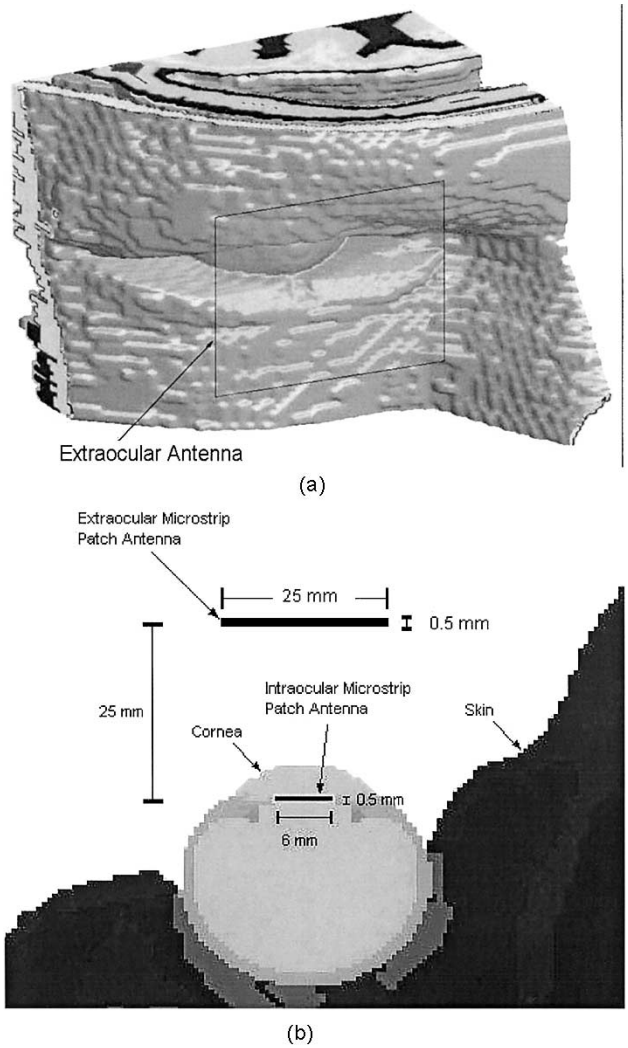

Fig. 3. Head model used in the FDTD computational domain. (a) 3-D rendering of the three-dimensional model. (b) Horizontal cross-sectional slice through the center of the eyeball.

IV. Experimental Setup

For coupling measurements in free space, both the antennas were fixed on a pair of clamps and were connected to an HP 8510C network analyzer. The extraocular and intraocular antennas were oriented on the same axis facing each other in their broadside direction. Coupling measurements as a function of free-space separation and angular separation were performed in both frequency bands at 1.45 and 2.45 GHz.

The effect of misalignment on the coupling performance of the link was also investigated. To this objective, the distance of separation between the antennas was maintained constant (at approximately 25 mm) and a set of coupling measurements were taken as a function of the angular separation between the two antennas. At each frequency band (1.45 and 2.45 GHz), two cases were considered for the coupling measurements. In the first case, the extraocular antenna was rotated along a path, which was symmetrical about the shorting post of the intraocular antenna, while in the second case, the rotational path was asymmetrical to the shorting post of the intraocular antenna.

To assess the performance of the data telemetry link in presence of the eyeball (with the intraocular antenna immersed in the eyeball), an eye phantom was realized by a thin plastic sphere filled with a liquid simulating the properties of the vitreous humor. To simulate the electrical properties of vitreous humor, a fluid with a composition of water and appropriate proportions of sugar and salt was developed. Two different vitreous humor simulant fluids were developed to closely simulate the electrical properties (dielectric constant and conductivity) of vitreous humor at 1.45 and 2.45 GHz . The electrical properties of the fluid were determined by using a coaxial probe and a technique described in [21].

To ensure stable position during measurements, this eye phantom was snugly fit into a circular hole cut out of a square styrofoam sheet. A slice was removed from the top of the eye phantom to make the right sized opening for immersing the encapsulated intraocular antenna. To prevent any contact with the fluid vitreous humor simulant in the eyeball, the intraocular antenna (along with the coaxial cable connecting it) was encapsulated in a thick plastic sheath. The extraocular and intraocular antennas were fixed on two supports and clamped on a vertical scaled bar. The encapsulated antenna was immersed into the eye phantom to the approximate depth required. With this setup, coupling measurements were taken as a function of separation between the extraocular and intraocular antennas.

V. Influence of the Eyeball on Intraocular Antenna Characteristics

When the encapsulated intraocular antenna is immersed in the eye phantom filled with humor simulant fluid, due to the dielectric loading effect, the antenna is de-tuned [22]. The resonant frequency gets lowered and the return loss degrades due to an inductive effect in its impedance characteristics. The dielectric loading effect is more pronounced at the higher frequency band of 2.45 GHz. Thus, for experimental measurements in the presence of the model, a new set of intraocular antennas had to be implemented, accounting for the inductive loading effect due to immersion in the eye phantom. The new intraocular antennas were designed so that they exhibit capacitive behavior at the desired extraocular antenna frequency in free space. To this end, the intraocular antennas, as shown in Fig. 2(a) and (b), were modified by altering the widths of the shorting posts to make them capacitive in free space. This ensured that when these modified intraocular antennas were immersed in the eye phantom, the inductive dielectric loading influence would re-tune them (resonant with good impedance matching) to the desired frequency of the extraocular antenna. Henceforth, in this study, these modified intraocular antennas are termed as redesigned intraocular antennas.

Fig. 4(a) and (b) shows the impedance characteristics of the redesigned intraocular antenna (in free space and after immersing in the eye phantom) and that of the transmitting antenna in the 1.45-GHz band. It is shown that, in free space, there is an offset of 15 MHz between the resonant frequencies of the redesigned intraocular antenna and the transmitting antenna. However, when the redesigned intraocular antenna is immersed in the eye phantom, its resonant frequency matches that of the transmitting antenna at 1.4 GHz. Similarly, Fig. 4(c) and (d) shows the impedance characteristics for the intraocular antenna

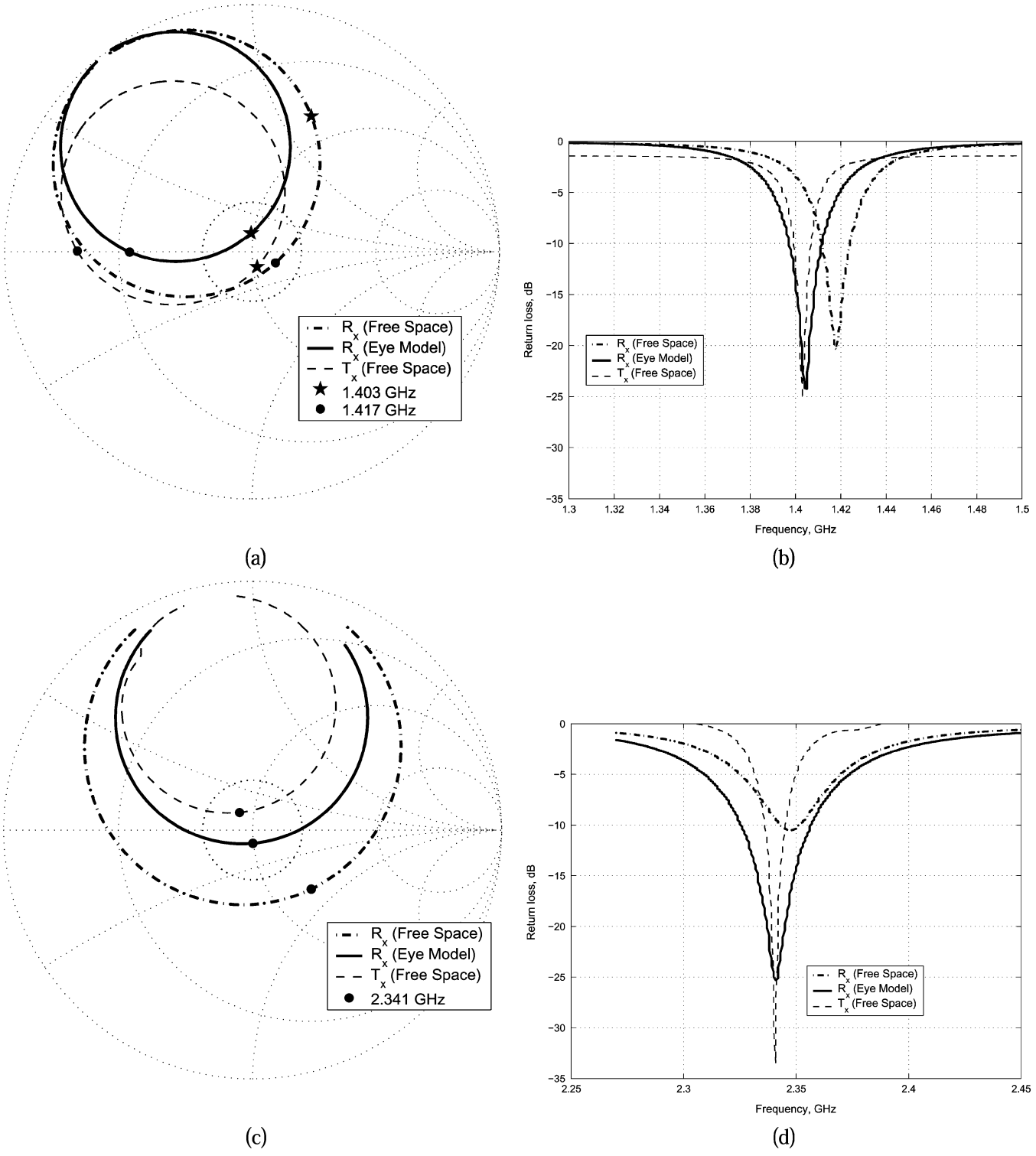

Fig. 4. Experimental measurements showing the influence of the eye model on the impedance characteristics of the intraocular antenna; While the redesigned intraocular antenna is de-tuned in free space, it resonates at the same frequency of the transmitting antenna when immersed in the eye model. (a) Smith-chart characteristics in the 1.45-GHz band. (b) Return-loss characteristics in the 1.45-GHz band. (c) Smith-chart characteristics in the 2.45-GHz band. (d) Return-loss characteristics in the 2.45-GHz band.

in the 2.45-GHz band. In this case, due to the pronounced effect of dielectric loading, the intraocular antenna was redesigned to exhibit substantial capacitive behavior in free space so that the inductive influence when immersed in the eye phantom leads to a good matching at the desired extraocular antenna frequency.

VI. Results and Discussion

A. Coupling Between the Two Antennas

Numerically, due to the length of the simulations, coupling was computed only for a fixed separation of 25 mm between

TABLE II
COUPLING PERFORMANCE AT A SEPARATION OF 25 mm AT BOTH FREQUENCY BANDS (1.45 AND 2.45 GHz)

Frequency band	Free Space (dB)		Eye Phantom (dB)	
	Num.	Exp.	Num.	Exp.
1.45 GHz	−41.5	−42.5	−34.6	−37.2
2.45 GHz	−28.9	−32.0	−27.4	−31.1

the extraocular and intraocular antennas. These computations were performed at both the frequency bands in free space, as well as in the presence of the eye model. Experimentally, both in free space and in the presence of the eye model, coupling was observed as a function of broadside separation between the two antennas at both frequency bands. Measurements with respect to angular separation (to determine the effect of misalignment) were obtained only in free space. Numerical and experimental coupling results were compared for the separation of 25 mm between the two antennas in free space and in the presence of the eye model.

In the 1.45-GHz frequency band, at a separation of 25 mm in free space, the numerically computed coupling was −41.5 dB and the experimentally observed value was −42.5 dB. When the intraocular antenna was embedded in the eye model, numerically computed coupling increased to −34.6 dB, while experimentally, the measured coupling was −37.2 dB. Numerical and experimental results are in close agreement, and the increase in coupling in the presence of the eye model suggests that the eye ball acts as a dielectric lens for the intraocular antenna and actually improves the coupling performance.

In the 2.45-GHz band, again at a separation of 25 mm between the antennas, in free space, the numerically computed coupling was −28.9 dB and, experimentally, it was observed to be −32.0 dB. In the presence of the eye model, there was a slight increase in coupling. Numerically, it increased to −27.4 dB, while the experimentally measured value was −31.1 dB. It is seen that, due to the dielectric lens effect of the eye ball, coupling at 1.45 GHz improved significantly by 4–6 dB, while at 2.45 GHz, the improvement was less, around 1–2 dB. Also, it is observed that, at a separation of 25 mm, coupling at 1.45 GHz is lower than that at 2.45 GHz. This may be attributed to the fact that, for the same sized antennas, at 1.45 GHz, the greater compactness deteriorates the antenna efficiency, thus degrading the coupling performance. The coupling performance at 25-mm separation is summarized in Table II.

Fig. 5(a) and (b) compares the coupling performance at both the frequency bands at a separation of 25 mm in free space and in the presence of the eye model. Numerically as well as experimentally, an improvement in coupling is observed (4–6 dB at 1.45 GHz and 1–2 dB at 2.45 GHz) when the intraocular antenna is immersed in the eye model. The discrepancy between the numerical and experimental frequencies of operation is due to the fact that the implemented antennas (for experimental results) operated at a lower frequency (as explained earlier in Section II). Besides this, as seen in Fig. 5(b), there is also a slight discrepancy between the experimentally obtained curves for free space and in the presence of the eye model. This is due to the fact that, for measurements in the presence of the eye model, the antennas

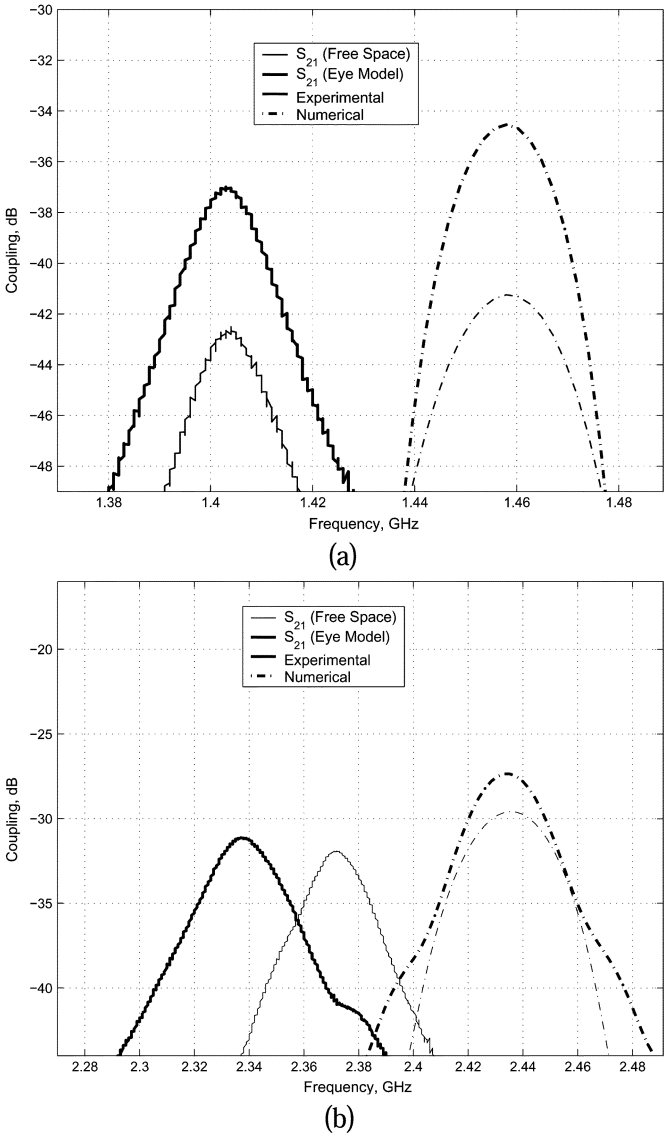

Fig. 5. Improvement in coupling performance at 25-mm separation (experimental and numerical) in the presence of the eye model. (a) 1.45 GHz. (b) 2.45 GHz.

were redesigned (as explained in Section V) and, on implementation, operated at a lower frequency than those in free space.

Fig. 6(a) and (b) compares the experimentally observed coupling as a function of the distance of separation both in free space, as well as in the presence of the eye model at 1.45 and 2.45 GHz, respectively. At 1.45 GHz, for all distances of separation examined, observed coupling with the intraocular antenna embedded in the eye model is higher than that in free space, while at 2.45 GHz, for separation less than 26 mm, coupling in the presence of the eye model is higher, but it falls below the corresponding free space values beyond 26 mm.

Fig. 7(a) and (b) shows measured coupling as a function of angular orientation between the two antennas for 1.45 and 2.45 GHz, respectively. At both frequency bands, when the extraocular antenna is rotated symmetrically with respect to the shorting post of the intraocular antenna (shown as the $\phi = 0^\circ$ case), the coupling is maximum at broadside and symmetric on either side of the broadside direction. For asymmetric rotation

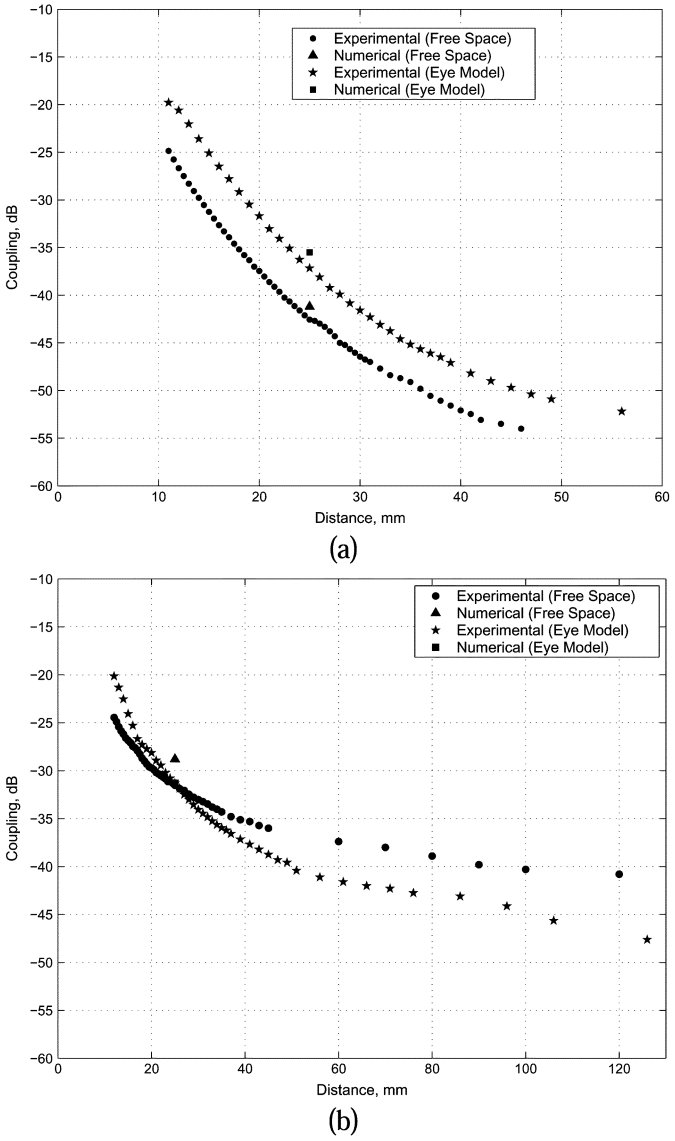

Fig. 6. Comparison of coupling in free space and in presence of the eye model as a function of separation. (a) 1.45 GHz. (b) 2.45 GHz.

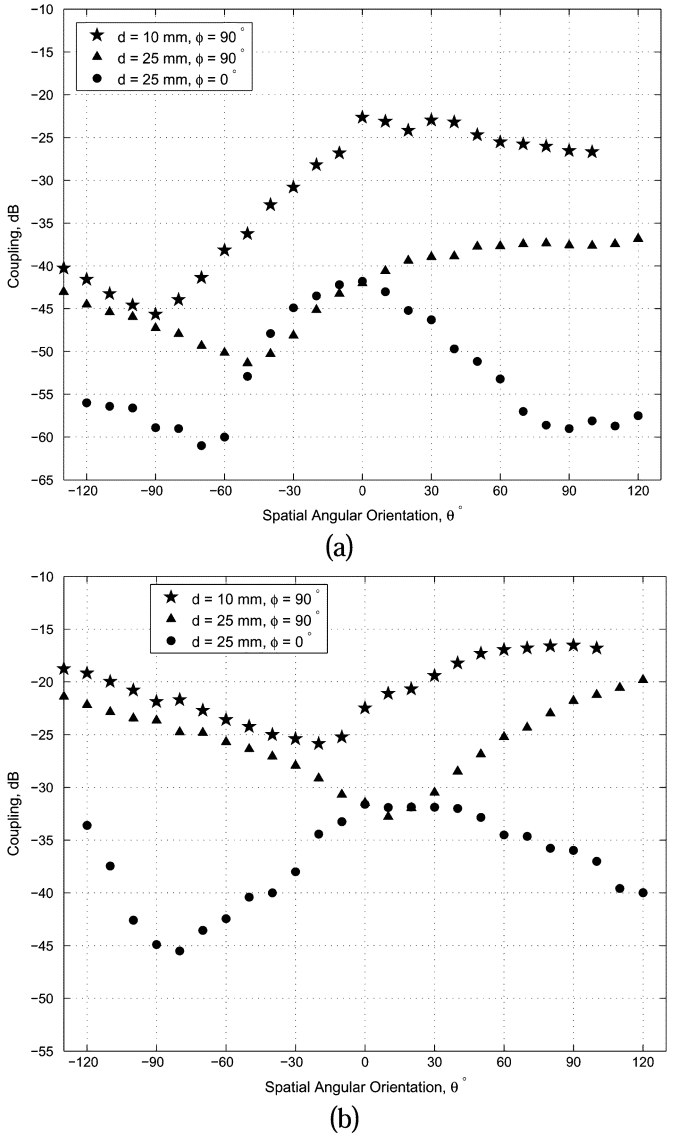

Fig. 7. Coupling as a function of angular separation at a fixed distance of 25 mm (for symmetrical and asymmetrical rotation of extraocular antenna with respect to the shorting post of intraocular antenna). (a) 1.45 GHz. (b) 2.45 GHz.

(shown as the $\phi = 90°$ case), coupling improves away from the broadside direction, thus indicating that with a particular orientation of the antennas, the wireless link can be made quite robust to misalignment.

We observed, as expected, that the coupling is very sensitive to the intraocular antenna's depth of immersion in the eye model. Moreover, the intraocular antenna (which has been redesigned to account for the dielectric influence) operates with good impedance characteristics for only a specific range of depth of immersion (for experimental measurements) and, therefore, its positioning at the proper depth in the eye model was essential to ensure good matching at the desired frequency.

B. SAR Computations

Electromagnetic energy gets deposited in the eye and surrounding head tissues due to the operation of the wireless data telemetry link. Computations to quantify the power deposited in terms of the SAR were performed at both frequency bands. As mentioned in Section I, due to the sensitivity of receiver architectures that can be employed (to further process the received signal from the intraocular antenna), the transmitter antenna is not expected to radiate more than 50 mW. Hence, the SAR values were normalized to a maximum transmitted power of 50 mW. Peak 1-g SAR values were calculated to determine compliance with the IEEE/ANSI stipulated guidelines.

TABLE III
COMPUTED SAR AT BOTH FREQUENCY BANDS (1.45 AND 2.45 GHz)

Frequency (GHz)	Peak 1-g (W/kg)
1.45	0.985
2.45	1.158

It is observed that maximum power deposition takes place in the forehead region for both frequency bands. This is attributed

to the fact that the radiating extraocular antenna is closest to the forehead in the head model. At 1.45 GHz, a computed peak 1-g SAR of 0.985 W/kg and, at 2.45 GHz, a peak 1-g SAR of 1.158 W/kg was observed, as summarized in Table III. Thus, at both frequency bands, for a maximum power transmitted of 50 mW, the SAR values do not exceed the IEEE/ANSI guidelines [15].

VII. Conclusion

An investigation of a data telemetry link for retinal prosthesis employing microstrip patch antennas has been performed and the feasibility of this novel approach is demonstrated both numerically and experimentally. In this study, the data telemetry link is established at two frequencies of 1.45 and 2.45 GHz by designing appropriately sized extraocular and intraocular patch antennas. Coupling performance of the link is examined both numerically and experimentally in free space, as well as with the intraocular antenna embedded in an eye phantom.

At a separation of 25 mm, in the frequency band of 1.45 GHz, experimentally, the coupling was measured to be -42.5 dB in free space, and it improved to -37.2 dB when the intraocular antenna was immersed in the eye phantom. At 2.45 GHz, the corresponding experimental free-space coupling was -32.0 dB, and it improved to -31.1 dB in the presence of the eye phantom. Numerical and experimental values agreed well for all cases at a separation of 25 mm. The results suggest that the eye ball acts as a dielectric lens and improves the coupling performance of the wireless link. Computed peak 1-g SAR at 1.45 GHz is 0.985 W/kg and, at 2.45 GHz, is 1.158 W/kg and, hence, are within the IEEE stipulated limit of 1.6 W/kg.

Improvement in the coupling performance due to the dielectric lens effect of the eyeball indicates that, for some biomedical applications, a microwave telemetry link can be established despite the high absorption of microwaves in the human body.

References

[1] A. Santos, M. Humayun, E. de Juan, R. Greenberg, M. Marsh, J. Klock, and A. Milam, "Preservation of the inner retina in retinitis pigmentosa," *Arch. Opthalmol.*, vol. 115, pp. 511–515, 1997.

[2] M. S. Humayun, E. de Juan Jr., J. D. Weiland, G. Dagnelie, S. Katona, R. Greenberg, and S. Suzuki, "Pattern electrical stimulation of the human retina," *Vis. Res.*, vol. 39, pp. 2569–2576, 1999.

[3] E. Margalit, M. Maia, J. D. Weiland, R. J. Greenberg, G. Y. Fujii, G. Torres, D. V. Piyathaisere, T. M. O'Hearn, W. Liu, G. Lazzi, G. Dagnelie, D. A. Scribner, E. de Juan, Jr., and M. S. Humayun, "Retinal prosthesis for the blind," *Survey Ophthalmol.*, vol. 47, no. 4, pp. 335–356, 2002.

[4] E. Zrenner, "Will retinal implants restore vision?," *Sci. Mag.*, vol. 295, pp. 1022–1025, Feb. 2002.

[5] S. C. DeMarco, G. Lazzi, W. Liu, J. D. Weiland, and M. S. Humayun, "Computed SAR and thermal elevation in a 0.25 mm 2-D model of the human eye and head in response to an implanted retinal stimulator: Parts I and II," *IEEE Trans. Antennas Propagat.*, vol. 51, pp. 2274–2295, Sept. 2003.

[6] R. Eckmiller, "Learning retina implants with epiretinal contacts," *Ophthalmic Res.*, vol. 29, pp. 281–289, 1997.

[7] M. V. Narayanan, J. F. Rizzo, D. Edell, and J. L. Wyatt, "Development of a silicon retinal implant: Cortical evoked potentials following focal stimulation of the rabbit retina with light and electricity," *Investigative Ophthalmol. Vis. Sci.*, vol. 35, p. 1380, 1994.

[8] E. Zrenner, A. Stett, S. Weiss, R. B. Aramant, E. Guenther, K. Kohler, K. D. Miliczek, M. J. Seiler, and H. Haemmerle, "Can subretinal microphotodiodes successfully replace degenerated photoreceptors?," *Vis. Res.*, vol. 39, no. 15, pp. 2555–2567, July 1999.

[9] Y. Chow and V. Y Chow, "Subretinal electrical stimulation of the rabbit retina," *Neurosci. Lett.*, vol. 225, pp. 13–16, 1997.

[10] R. A. Normann, E. M. Maynard, P. J. Rousche, and D. J. Warren, "A neural interface for a cortical vision prosthesis," *Vis. Res.*, vol. 39, no. 15, pp. 2577–2587, July 1999.

[11] R. E. Marc and B. W. Jones, "Retinal remodeling in inherited photoreceptor degenerations," *Mol. Neurobiol.*, vol. 28, no. 2, pp. 139–148, Oct. 2003.

[12] M. Ghovanloo and K. Najafi, "A high-rate frequency shift keying demodulator chip for wireless biomedical implants," in *Proc. Int. Circuits and Systems Symp.*, vol. 5, May 2003, pp. 25–28.

[13] K. Gosalia, P. Brown, W. Liu, and G. Lazzi, "FDTD investigation of a microwave link for data telemetry in retinal prosthesis applications," in *Int. Antennas and Propagation Symp. Dig.*, vol. 1, 2002, pp. 807–810.

[14] K. Gosalia, W. Liu, J. Weiland, M. S. Humayun, and G. Lazzi, "An investigation of the coupling between extremely compact microstrip patch antennas in a link for biomedical implants," presented at the Int. URSI Antennas and Propagation Symp., 2003.

[15] *Safety Levels with Respect to Human Exposure to Radio Frequency Electromagnetic Fields, 3 kHz to 300 GHz*, IEEE Standard C95.1-1999, 1999.

[16] C. A. Balanis, *Antenna Theory: Analysis and Design*, 2nd ed. New York: Wiley, 1997.

[17] I. J. Bahl and P. Bhartia, *Microstrip Antennas*. Dedham, MA: Artech House, 1980.

[18] K. L. Wong, *Compact and Broadband Microstrip Antennas*. New York: Wiley, 2002.

[19] D. Sullivan, *Electromagnetic Simulation Using the FDTD Method*. Piscataway, NJ: IEEE Press, 2000.

[20] G. Lazzi, O. P. Gandhi, and D. Sullivan, "Use of PML absorbing layers for the truncation of the head model in cellular telephone simulations," *IEEE Trans. Microwave Theory Tech.*, vol. 48, pp. 2033–2039, Nov. 2000.

[21] Y. Wei and S. Sridhar, "Technique for measuring the frequency dependent complex dielectric constants of liquids up to 20 GHz," *Rev. Sci. Instrum.*, vol. 60, no. 9, pp. 3041–3046, Sept. 1999.

[22] I. J. Bahl, P. Bhartia, and S. S. Stuchly, "Design of microstrip antennas covered with a dielectric layer," *IEEE Trans. Antennas Propagat.*, vol. AP-30, pp. 314–318, Mar. 1982.

Keyoor Gosalia (S'01) received the B.E. degree in electronics from Sardar Patel University, Gujarat, India, in 1999, the M.S. degree in electrical engineering from North Carolina State University, Raleigh, in 2001, and is currently working toward the Ph.D. degree in electrical engineering at North Carolina State University.

His research interests include application of the FDTD method for bioelectromagnetics, novel design techniques for electrically small microstrip patch and wire antennas, and planar ultra-wide-band antenna systems for improving multiple-input–multiple-output (MIMO) channel capacity.

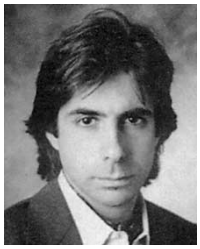

Gianluca Lazzi (S'94–M'95–SM'99) was born in Rome, Italy, on April 25, 1970. He received the Dr.Eng. degree in electronics from the University of Rome "La Sapienza," Rome, Italy, in 1994, and the Ph.D. degree in electrical engineering from the University of Utah, Salt Lake City, in 1998.

He has been a consultant for several companies (1988–1994), a Visiting Researcher with the Italian National Board for New Technologies, Energy, and Environment (ENEA) (1994), a Visiting Researcher with the University of Rome "La Sapienza" (1994–1995), and a Research Associate (1995–1998) and Research Assistant Professor (1998–1999) with the University of Utah. He is currently an Associate Professor with the Department of Electrical and Computer Engineering, North Carolina State University (NCSU), Raleigh, where, from 1999 to 2003, he was an Assistant Professor. He has authored or coauthored over 80 international journal papers or conference presentations on FDTD modeling, dosimetry, and bioelectromagnetics. He is listed in *Who's Who in the World*, *Who's Who in America*, *Who's Who in Science and Engineering*, the *Dictionary of International Biographies*, and the 2000 *Outstanding Scientists of the 20th Century*.

Dr. Lazzi is an associate editor for the *IEEE Antennas and Wireless Propagation Letters*. He is the vice chair of Commission K (Electromagnetics in Biology and Medicine), U.S. National Committee of the International Union of Radio Science (URSI). He was the recipient of the 2003 ALCOA Foundation Engineering Research Achievement Award, a 2003 NCSU Outstanding Teacher Award, the 2003 NCSU Alumni Outstanding Teacher Award, a 2001 National Science Foundation (NSF) CAREER Award, a 2001 Whitaker Foundation Biomedical Engineering Grant for Young Investigators, a 1996 International Union of Radio Science (URSI) Young Scientist Award, and the 1996 Curtis Carl Johnson Memorial Award for the best student paper presented at the 18th Annual Technical Meeting of the IEEE Bioelectromagnetics Society (IEEE BEMS).

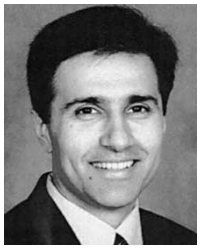

Mark Humayun (M'97) received the M.D. degree from the Duke University Medical School, Durham, NC, in 1989, and the Ph.D. degree in biomedical engineering from the University of North Carolina, Chapel Hill, in 2001.

He served a residency in ophthalmology at the Duke Eye Center and fellowships with the Retinovascular Center, Johns Hopkins Hospital, and in vitreoretinal surgery with the Johns Hopkins Medical Institution. From 1995 to 2001, he was an Assistant Professor of ophthalmology with the Johns Hopkins Wilmer Eye Institute. He is currently Professor of Ophthalmology with the Keck School of Medicine, University of Southern California, Los Angeles, and Associate Director of Research with the Doheny Retina Institute, Los Angeles, CA, where he provides patient care while developing innovative techniques and diagnostics to treat blinding retinal disorders. His quest to find a cure for currently untreatable blinding retinal diseases led him to become one of the primary creators of the intraocular retinal prosthesis that was recently implanted into the first patient in a Food and Drug Administration (FDA) investigational device study. In August 2001, he joined the Doheny Retina Institute, Doheny Eye Institute, where he holds three appointments: ophthalmology, biomedical engineering and cell and neurobiology. His research has focused on microelectronic solutions for severe retinal disease.